Upstream Polarimetry with 4-Magnet Chicane

N. Meyners, V. Gharibyan, K.P. Schüler
DESY, Hamburg, Germany

We have extended an earlier polarimeter study to evaluate the merits of a 4-magnet chicane spectrometer for upstream Compton polarimetry. This spectrometer configuration has been advocated for downstream polarimetry as an effective separator of Compton electrons from disrupted beam backgrounds. The chicane spectrometer is also advantageous for upstream polarimetry, as a single laser wavelength in the visible will be sufficient to cover all possible beam energies.

1. INTRODUCTION AND OVERVIEW

In an earlier study [1], we had worked out a laser-based Compton polarimeter design for the TESLA machine [2]. This design is an upstream polarimeter configuration with a laser beam crossing ahead of the e+e- detector, at the end of a long straight section in the TESLA beam delivery system (BDS). Since the entire BDS layout of the cold machine is currently being reconfigured in the context of the ILC, we have begun to explore the chicane design of the downstream polarimeter, which is being studied at SLAC [3], also for the upstream polarimeter location. Most major aspects of our earlier study, except for the spectrometer, remain valid. In particular, we retain the TTF-style laser developed by Max-Born-Institute [4], as it is well adapted to the particular bunch and pulse structure of the cold machine.

2. 4-MAGNET CHICANE

2.1. General Layout and Properties

We start out with the simple chicane layout indicated in fig. 1, with all four dipoles D1-D4 having the same length of 2 m, identical field integral of 0.833 Tm, and a transverse momentum kick of 0.250 GeV/c. The horizontal width of the good field region of the inner two dipoles is 20 cm, to accommodate a maximum dispersion of 110 mm for the lowest expected beam energy of 45.6 GeV for the Giga-Z option. The laser beam enters and exits between the inner two dipoles, which must be separated by some 8 meters for a vertical beam crossing angle of 10 mrad. A possible optical arrangement for this will be shown in the next subchapter.

Compton electrons generated at the laser IP at mid-chicane will propagate essentially along the electron beam direction inside a narrow angular cone with a maximum half angle of $\vartheta_e^{max} = 2\omega_0/m \sim 10\ \mu$rad for a green laser with a photon energy $\omega_0 = 2.3$ eV. The thrird dipole D3 will then fan out the Compton electron spectrum, while the fourth dipole can be used to restore the angular direction, if it has sufficient horizontal width. It can be shown [5] that the maximum horizontal deflection of the Compton electrons, corresponding to the Compton edge of minimum energy, is independent of beam energy and given by $x_{max} = 4\omega_0 p_T L_{sep}/m^2$. With a center to center separation $L_{sep} = 20$ m between D3 and D4, one obtains a maximum offset from the beam of $x_{max} = 17.8$ cm for a green laser and $p_T = 0.250$ GeV/c.

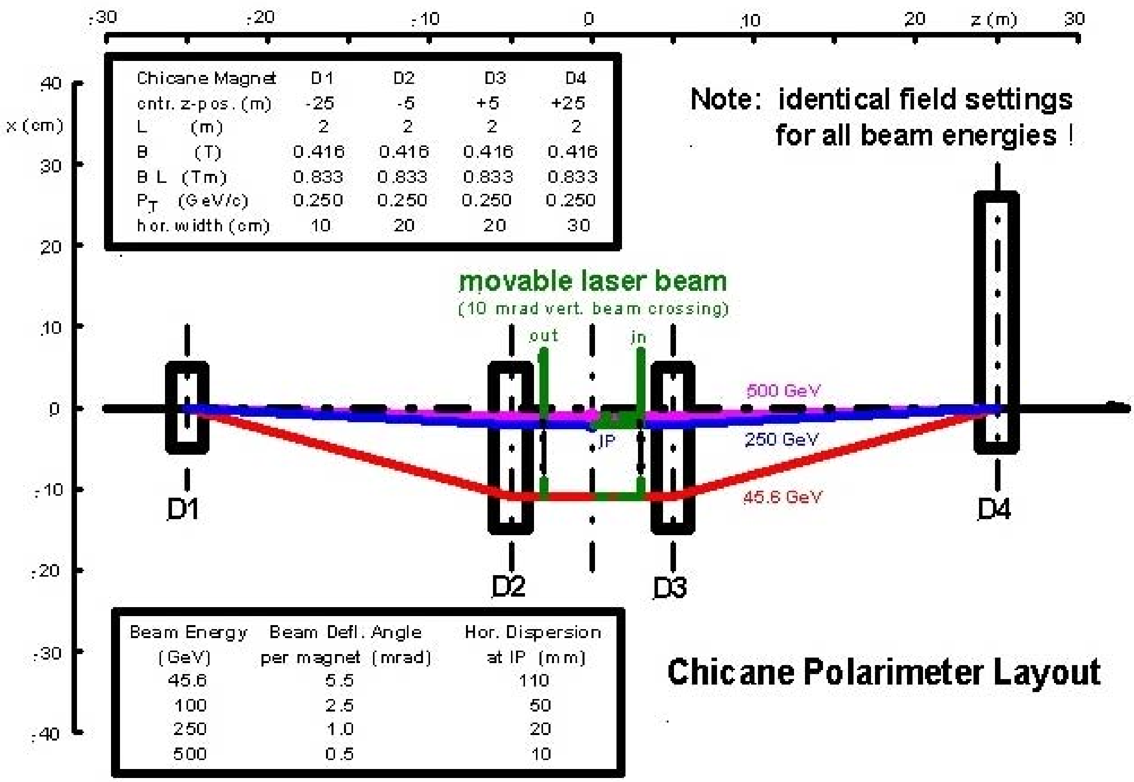

Figure 1: Schematic Chicane Layout

2.2. Movable Laser Beam

As we plan to operate the chicane with a constant field setting over a large range of beam energies, we have to shift the laser beam so that it can interact with the electron beam over a corresponding large range of dispersions. Such a movable laser beam can be accommodated with a movable mirror/lens assembly, as shown in fig. 2, that rides on top of the electron beam in a separate chamber. The optics chamber and the electron beam pipe, both of which have rectangular cross sections, connect through an aperture near the Compton IP. There is an identical arrangement for the extraction of the laser beam, which is desirable to analyze the intensity and polarization of the laser light.

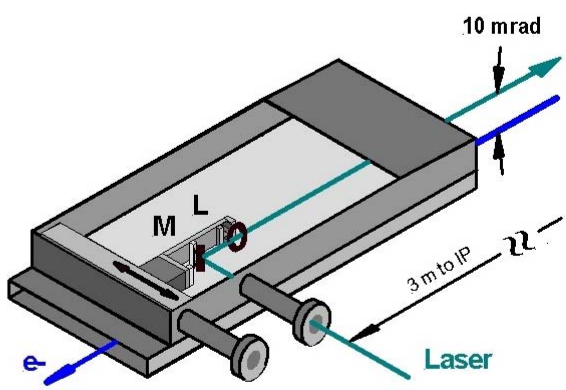

Figure 2: Movable Laser Beam

2.3. Vacuum Chambers

The form and size of the vacuum chambers is largely dictated by trajectories of the beam and the Compton electrons. Furthermore, variations in transverse dimensions should be smooth, in order to minimize wakefield effects. Fig. 3 shows the overall layout and Fig. 4 shows some details of the central segment where the optics chambers connect with the electron beam pipe. The wakefield effects caused by these apertures will have to be studied.

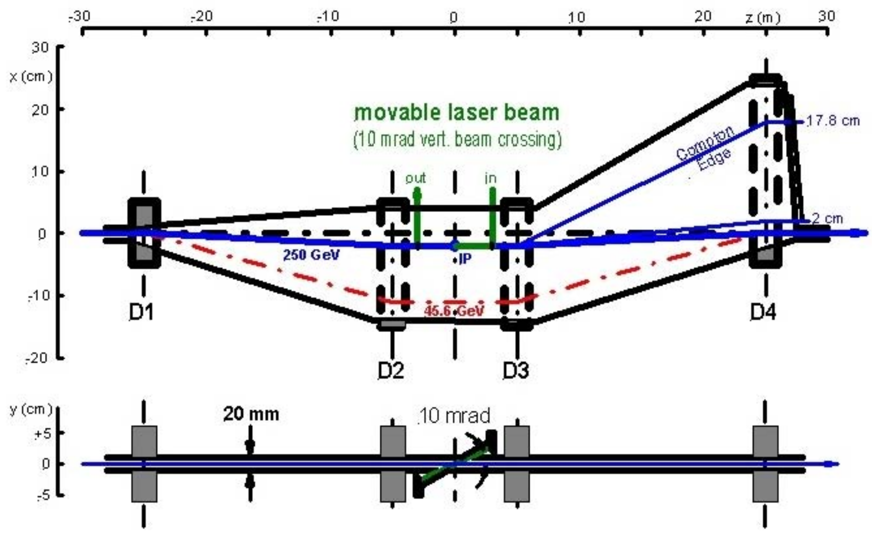

Figure 3: Vacuum Chamber Overview

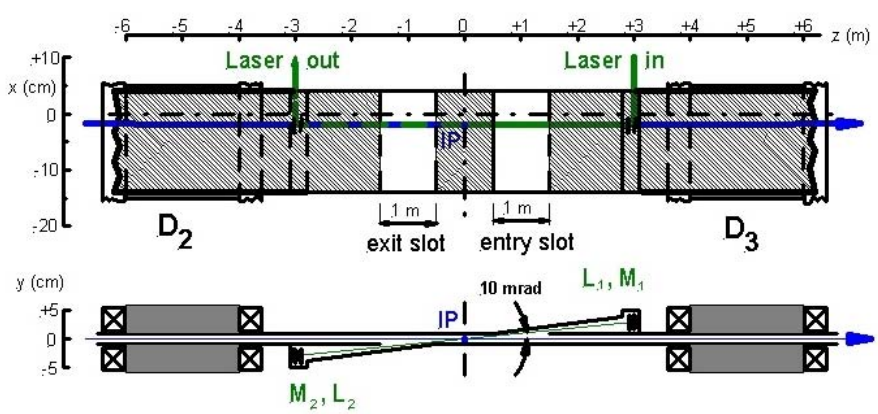

Figure 4: Vacuum Chamber Detail

2.4. Electron Detector

The electron detector behind the last dipole is a gas Cerenkov hodoscope with 20 identical channels, which are staggered along the beam direction, as shown in fig. 5, to accommodate the phototubes and the tapered vacuum chamber. The individual channels have a rectangular cross section (10 mm wide x 20 mm high) and are filled with C_4F_{10} gas, which has an electron threshold of 10 MeV.

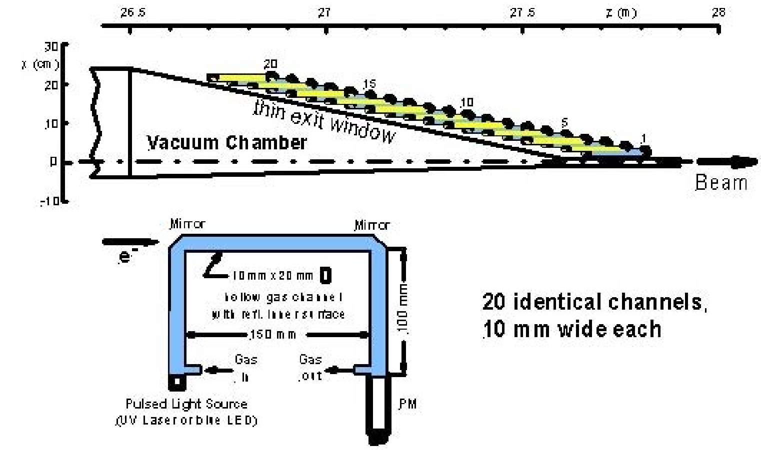

Figure 5: Electron Detector Hodoscope

2.5. Synchrotron Radiation and Emittance Growth

For an initial assessment of synchrotron radiation levels, we begin again with our simplified chicane geometry, where all four magnets have an identical length of 2 m., as shown in fig. 6. While none of the synchrotron radiation fans has a direct line of sight into the detector, one still has to worry about indirect radiation scattering off the walls of the vacuum chamber. At higher beam energies, it may be necessary to employ movable jaws to shield against such background.

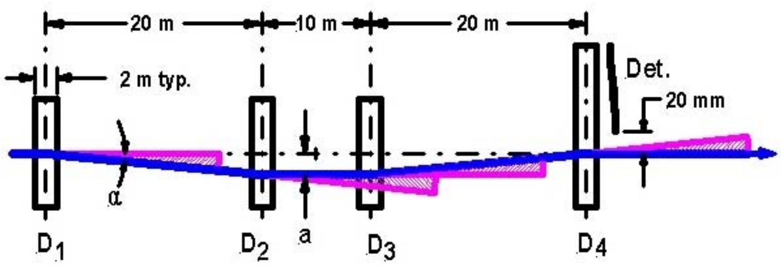

Figure 6: Synchrotron Radiation Geometry

The radiation levels expected for the simplified geometry are listed in table 1.

E [GeV]	α [mrad]	a [mm]	ΔE/el. [MeV]	ΔE/bunch [mJ] (*)	ΔE/sec [kJ] (**)	total power [kW]
			-------------------- per magnet		-----------------	(4 magnets)
45.6	5.5	110	0.9	3	0.04	0.16
100	2.5	50	4.4	14	0.20	0.80
250	1.0	20	27.5	88	1.24	4.96
500	0.5	10	110.0	352	4.96	19.85

(*) 2×10^{10} el./bunch (**) 5 x 2,820 = 14,100 bunches/sec

Table 1: Synchrotron Radiation Levels for the Geometry of Fig. 6

By increasing the length of the magnets [6] so that the outer dipoles D1 and D4 each have a length of 3 m, while the inner dipoles D2 and D3 increase to a length of 6 m each, it is possible to reduce the radiated power to 50% of the values shown in the table. The associated emittance growth for this stretched chicane geometry has been evaluated with DIMAD tracking by Mark Woodley [7]. For a beam energy of 250 GeV and a dispersion of 20 mm, he finds an emittance dilution of 0.49%, which is still acceptable. For higher beam energies though, we would have to reduce the field setting of the chicane; e.g. with a dispersion of 5 mm at 500 GeV, which corresponds to half the field setting assumed in table 1, the emittance dilution is only 0.07%.

2.6. Compton Event Simulations

We have produced a new and rather flexible simulation code that will generate spin-dependent Compton event distributions with a large number of externally controllable parameters. As to be expected, the results of these simulations are very similar to those reported in our earlier study [1].

Ch. #	x [mm]	N+	N-	A	Rate × A²	Rate [MHz]	dP/P [%]
1	25	60,682	23,368	-0.444	0.337	1.710	0.228
2	35	45,868	17,348	-0.451	0.262	1.287	0.260
3	45	35,673	16,012	-0.380	0.152	1.052	0.335
4	55	28,337	16,029	-0.277	0.069	0.903	0.486
5	65	22,996	16,056	-0.151	0.019	0.813	0.924
6	75	18,333	17,876	-0.013	0.000	0.737	11.521
7	85	15,248	18,744	0.103	0.007	0.692	1.466
8	95	12,025	19,818	0.245	0.039	0.648	0.646
9	105	9,881	20,480	0.349	0.075	0.618	0.473
10	115	7,815	21,525	0.467	0.130	0.597	0.370
11	125	6,246	21,961	0.557	0.178	0.574	0.324
12	135	4,849	22,795	0.649	0.237	0.562	0.289
13	145	3,479	23,315	0.740	0.299	0.545	0.266
14	155	2,385	23,821	0.818	0.357	0.533	0.250
15	165	1,346	24,171	0.895	0.416	0.519	0.238
16	175	457	20,900	0.957	0.398	0.435	0.249
17	185	0	0				

Table 2: Some Simulation Results

The example demonstrated in table 2 applies to the standard configuration with a beam energy of E_0 = 250 GeV, a green laser with ω_0 = 2.33 eV, a luminosity $L = 1.5 \times 10^{32}/cm^2/sec$, 0.5×10^6 generated Compton events per laser polarity, and the chicane and detector configuration as described in this paper. The overall statistical error for a measurement time of dT = 1 sec is dP/P = 0.082 %. The performance for other beam energies is similar.

2.7. Remaining Issues

The wakefield effects associated with the geometry of the vacuum chambers and in particular with the insertion and exit apertures for the laser beam need further study. This work is in progress. Also the effect of synchrotron radiation bouncing off the walls of the vacuum chamber needs to be evaluated. Eventually, there is a lot of conventional engineering work of magnets, vacuum chambers, optics etc. to be done.

3. SUMMARY AND CONCLUSIONS

We have begun to examine the 4-magnet chicane geometry for upstream Compton polarimetry at the ILC. With sufficient clearance of some 8 meters between the central dipole magnets, it is possible to retain all essential features and results of our earlier study, which had been tailored to the TESLA BDS configuration. With the chicane it is possible to do Compton polarimetry at all beam energies of interest with a single laser wavelength in the visible, which simplifies matters considerably. In order to eliminate any significant emittance growth at beam energies near 500 GeV, the field setting of the chicane magnets should be reduced from the standard operating point. Although this will reduce the broad range of the Compton spectrum that can be detected, it will still retain the important low-energy part, which is essential for polarimetry.

References

[1] V. Gharibyan, N. Meyners, K.P. Schüler, LC-DET-2001-047, see http://www.desy.de/~lcnotes

[2] TESLA TDR (2001)

[3] M. Woods and K. Moffeit, SLAC-PUB-10669 (2004), LCWS-04, Paris, France, 2004;
K. Moffeit, MDI workshop at SLAC, Jan. 2005.

[4] S. Schreiber et al., Nucl. Instr. Meth. A 445 (2000) 427.

[5] W. Oliver, MDI workshop at SLAC, Jan. 2005.

[6] K. Moffeit and R. Arnold, private communication.

[7] M. Woodley, private communication.